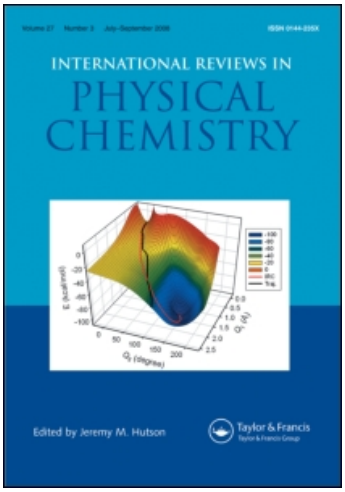

International Reviews in Physical Chemistry
Publication details, including instructions for authors and subscription information:
http://www.informaworld.com/smpp/title~content=t713724383

Orientation effects in electron transfer collisions

Philip R. Brooks[a]
[a] Department of Chemistry and Rice Quantum Institute, Rice University, Houston, Texas, USA

To cite this Article Brooks, Philip R.(1995) 'Orientation effects in electron transfer collisions', International Reviews in Physical Chemistry, 14: 2, 327 — 354
To link to this Article: DOI: 10.1080/01442359509353313
URL: http://dx.doi.org/10.1080/01442359509353313

INTERNATIONAL REVIEWS IN PHYSICAL CHEMISTRY, 1995, VOL. 14, NO. 2, 327–354

Orientation effects in electron transfer collisions

by PHILIP R. BROOKS
Department of Chemistry and Rice Quantum Institute, Rice University, Houston, Texas 77251, USA

... these atoms move in the infinite void, separate one from another and differing in shapes, sizes, position and arrangement; overtaking each other they collided, and some are shaken away in any chance direction, while others, becoming intertwined one with another according to the congruity of their shapes, sizes, positions, and arrangements, stay together and so effect the coming into being of compound bodies. (Simplicius)

The influence of molecular orientation upon electron transfer has been probed with oriented target molecules in crossed molecular beams. Electron transfer frequently occurs in thermal energy reactive collisions, but at thermal energies charged species can rarely escape their mutual Coulomb attraction, and only neutral products are formed. By increasing the collisional energy to a few eV, the charged species can be separated, and the role of orientation on the electron transfer process can be probed. Collisional ionization of fast ($\approx$ 3–20 eV) *neutral* K atoms has been observed for a variety of symmetric top molecules, such as CH_3I, which were *oriented* in a molecular beam prior to collision. In every case studied so far, the heads/tails orientation of the molecule drastically affects the overall probability of ion production. Electron transfer is the first step in ion production; in the second step the ions must get away from one another once formed. Both of these steps can depend on orientation, and the experiments probe the combination of the two. At energies a few volts beyond the threshold, many of the negative ions studied break apart and the orientation dependence seems mainly to be determined by how the ions get away from one another. But the thresholds themselves are orientation dependent, and for the reaction $K + CF_3Br$ the threshold for the *heads* (Br-end) orientation is below the threshold for anion fragmentation. The dominant orientation dependence is mostly in the entrance channel, and for this case we believe the electron is preferentially transferred to the Br end of the molecule.

1. Introduction

Molecular orientation is thought to play a crucial role in many collisional processes ranging from photoionization to chemical reaction. Usually processes involve a statistical distribution of orientations, and information about orientational requirements must be inferred from indirect experiments. But over the last 25 years or so, two methods have been developed for orienting molecules prior to collision: [1] orientation† by state selection in inhomogeneous electric fields which will be discussed here, and 'brute force' orientation of polar molecules in extremely strong electric fields [2]. Several chemical reactions have been studied with one of the reagents oriented prior to collision [1, 2].

† We differentiate between *orientation*, in which one end of a molecule may be distinguished from the other end, and *alignment* or *polarization* which can be induced optically (see [1 (*b*)]) where the plane of rotation can be selected, but one end of the molecule cannot be distinguished from the other end.

0144-235X/95 $10·00

Thermal energy chemical reactions are thought to be greatly affected by the orientation of the molecule, and direct observation using oriented molecules confirms these beliefs. The oriented molecule experiments have so far involved reactions which can be thought of as proceeding via an electron transfer. Reactions involving electron transfer are ubiquitous in chemistry and biology, but under normal circumstances (thermal energies) very few neutral species react to form ions because reactions are rarely energetic enough to cause the intermediate ions to separate as charged species. Transient ions thus normally recombine to form a salt, but if the initial energy is increased a bit the ions can be observed and the effect of molecular orientation on the electron transfer process can be probed more directly. In this article we shall discuss electron transfer collisions occurring in the intermediate region of a few eV where ions can be detected and where the processes are still expected to be similar to those obtaining at thermal energies.

2. Theoretical aspects of electron transfer

Electron transfer can occur when ionic and covalent states of the same symmetry have the same energy. Coupling between these states results in an avoided crossing of the diabatic covalent and ionic potential energy surfaces [3] as shown in figure 1 for the *atomic* system, $Na + I \rightarrow Na^+$ at I^-. At internuclear distances near the bond distance in the stable NaI molecule, r_c, the system is highly polar, Na^+I^-, and bonding is largely described by an ionic potential. The ionic salt molecule dissociates to give neutral atoms [4], so at large distances the molecule is best described by a covalent potential. At r_c these zeroth-order (diabatic) ionic and covalent curves appear to cross but a dissociating molecule must make a smooth transition from the ionic to covalent potential. For states of the same symmetry, the crossing is avoided by the adiabatic potentials, shown in figure 2, which result from solution of the two-state Schrödinger equation using the Born–Oppenheimer approximation. The adiabats, ε_1 and ε_2 are given in terms of the diabats by

$$\varepsilon_i = 1/2\{H_{11} + H_{22} \pm [(H_{11} - H_{22})^2 + 4H_{12}^2]^{1/2}\}. \tag{1}$$

The adiabatic curves resulting from ionic–covalent coupling do not cross, as shown in figure 2, and the character of the system changes smoothly from covalent at long range to ionic at short range.

The behaviour of a colliding system at the avoided crossing depends on the speed with which the crossing is traversed, as well as the separation and slopes of the adiabatic curves. If the atoms approach slowly enough on the covalent curve, the uncertainty principle allows the energy to be relatively well-defined, and the system stays on the lowest, adiabatic curve. This adiabatic process results in what we loosely call an electron 'jump'. On the other hand, if the atoms approach at high speed and traverse the crossing quickly, the energy will be less well-defined and it is possible that the system will remain on the diabatic curve (making a non-adiabatic or *diabatic* crossing) and will continue to be described by the covalent potential. (The diabatic crossing represents a 'hop' from one adiabatic potential curve to the other, but the electron stays on the atom and does not jump.)

The probability of a diabatic hop, P_d, is given to good approximation by the Landau–Zener relation [3],

$$P_d \approx \exp(-\kappa/v), \tag{2}$$

where $\kappa = (2\pi H_{IC})^2/h\Delta S$, and $\Delta S = |\partial E_I/\partial r - \partial E_C/\partial r|$, v is the speed, and H_{IC} is the

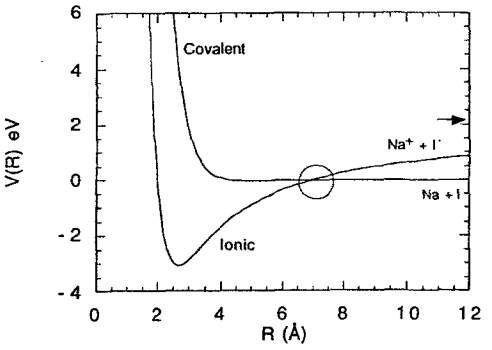

Figure 1. Diabatic potential curves for NaI. The arrow denotes the asymptotic energy of the ionic system.

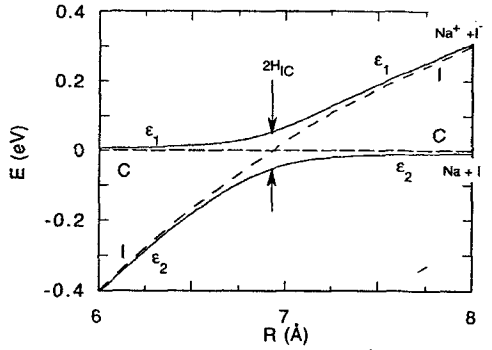

Figure 2. Adiabatic potential curves (ε_1 and ε_2) for the Na + I system near the diabatic curve crossing circled in figure 1. The diabatic ionic (I) and covalent (C) curves are shown as dashed curves. ($H_{IC} = 0{\cdot}05$ eV (Baede 1975).)

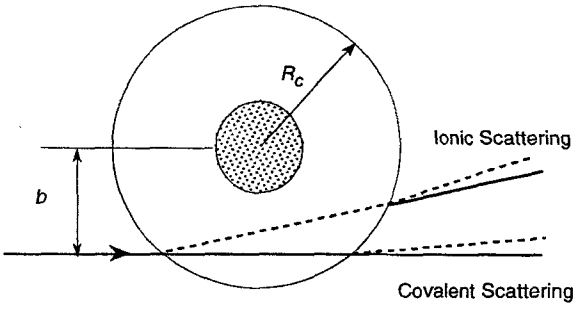

Figure 3. Simplified picture of atom–atom collisional ionization with crossing distance R_c. Heavy solid lines represent trajectories of neutral systems. At the first crossing ($r = R_c$) some fraction ($1 - P_d$) of trajectories make adiabatic transitions and are represented by dashed lines (ion pairs). Those making diabatic transitions remain neutral and continue their flight relatively unaffected. Each of these trajectories then encounters $r = R_c$ again, and again each trajectory can make an adiabatic or diabatic transition, resulting in ion pairs or neutrals depending on the trajectory. The ultimate production of ions requires one transition to be diabatic, and one to be adiabatic, in either order. The inner circle represents the repulsive core.

matrix element in the Hamiltonian that couples the two states. For the simplest crossing of an ionic curve with a covalent curve, the slope, of the covalent potential can be regarded as zero with zero energy compared to the separated atoms. The crossing radius is given approximately by the condition that $V(r_c)_{ionic} = V(r_c)_{covalent} = \Delta E_0 - e^2/r_c$, or

$$r_c = e^2/\Delta E_0, \tag{3}$$

where $\Delta E_0 = IP - EA$, the difference between the ionization potential of the donor (Na) and the electron affinity of the acceptor (I). $\Delta S = (e/r_C)^2$ and

$$\kappa = (4\pi^2 e^2/h)[H_{IC}(r_c)/\Delta E_0]^2. \tag{4}$$

Thus from equation (2) low speeds or large κ (large H_{IC} or large separation between the curves) gives a small P_d, and the probability of a diabatic 'hop' between potential curves is low. Under these circumstances the crossing is *adiabatic* and the system smoothly changes from a covalent to an ionic description. In this process the electron jumps from the Na atom to the I atom.

A complete collision requires the crossing to be traversed twice, once on the way in and once on the way out, as shown in figure 3. In order to produce ions starting with neutrals, the atomic system must traverse one crossing adiabatically, and the other diabatically. For the *atomic* system shown in figures 1–3, the two crossings are identical, and the overall probability of ionization is $P = (1 - P_d)P_d$. If the electron jumps at the first crossing the ions interact in close proximity to one another, leading to 'ionic scattering'. If the first crossing is diabatic, the close proximity encounter occurs between weakly interacting neutrals leading to 'covalent scattering', and the difference can be resolved in the differential scattering cross-section. This has been extensively and very nicely reviewed [3].

For atom–*molecule* collisions the situation is much more 'interesting'. Many more dimensions need to be taken into consideration and the interaction is likely to be dependent upon the orientation. This is shown schematically in figure 4, where the radius of the second crossing is shown to be different from of the first. Even a minute change in crossing distance can have a profound influence on the dynamics because the coupling matrix element, H_{12}, depends exponentially [3, 5] on r_c and the Landau–Zener (LZ) probability depends exponentially on H_{12}! Moreover, the internal state of the molecule can change between the crossings and the second crossing might be a crossing between surfaces quite different from those of the original system. This has been called 'bond stretching' in the earlier work [3].

As an example of how the internal state of the molecule influences the crossing, consider the effect of adding an electron to a diatomic molecule, such as Br_2. As shown in figure 5, the negative ion is less tightly bound than the neutral, and attachment of the electron (at fixed internuclear distance) results in a negative ion formed in a highly excited vibrational state. Following the electron jump, the Br nuclei begin to move apart which *increases* the apparent electron affinity of the Br_2. According to equation (3) this increases the crossing radius, decreases the ionic–covalent interaction, and greatly enhances the probability of the system making a diabatic transition. Since vibration of Br_2^- is expected to be periodic, the electron affinity and crossing radius will vary with time, and the electron transfer probability at the second crossing will depend on the time required (i.e., on the speed) for the atomic ion to arrive, as observed experimentally [6]. This effect has been referred to as 'bond stretching'. In the extreme limit of bond stretching, complete dissociation of the molecular ion may occur between the crossings, leaving only the atomic ions to undergo a diatomic crossing. This is discussed for

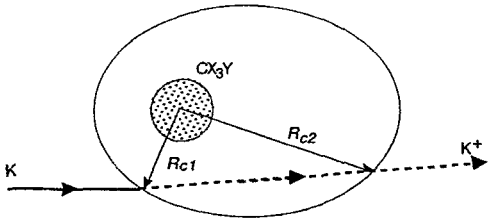

Figure 4. Simplified picture of atom–*molecule* collisional ionization. (Only the ionic scattering is shown.) The inner circle represents some repulsive core. The molecule is not spherical, and the crossing radii can differ as shown.

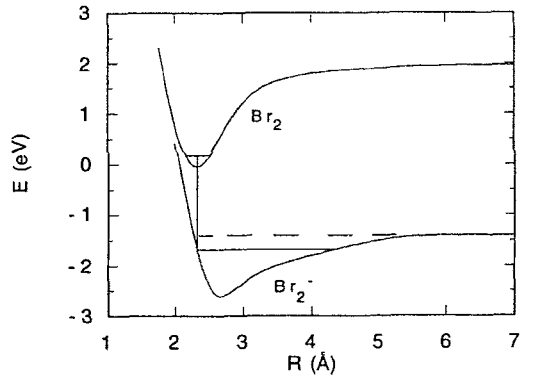

Figure 5. Potential curves for Br_2 and Br_2^-.

unoriented molecules in [3], and will be further discussed for oriented molecules in section 4.

3. Experimental aspects

Collisions are studied between neutral potassium atoms accelerated to energies ≈ 3–25 eV and molecules oriented in space. The orientation of the molecule can be changed so that one end of the molecule or the other can be presented to the incoming K atom. Positive ions formed in the collision are detected by one of two particle multipliers, depending on the orientation, and pulse counted. The apparatus is schematically shown in figure 6. Details concerning the construction may be found elsewhere [7].

3.1. *Oriented molecule beam*

A beam of RX molecules is formed by supersonic expansion of a neat (10% RX/90% He mixture)† from nozzle N, collimated in the skimmer and modulated by a rotating chopper wheel contained in a buffer chamber. The beam then enters an inhomogenous electrostatic field which passes the molecules which are in quantum states which correspond to the 'right' orientation with respect to a laboratory direction.

† Operating conditions changed during the course of the experiments. Values in brackets are those of Xing.

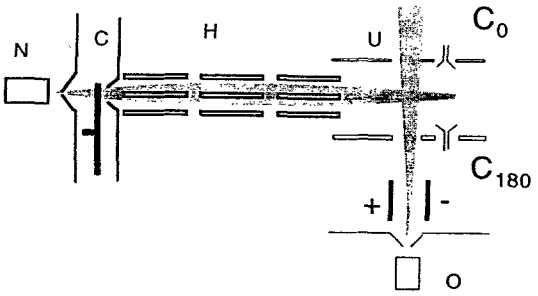

Figure 6. Schematic view of apparatus. N-nozzle source for RX beam, C = beam chopper, H = hexapole electric field state selector, U = uniform electric field, O = fast atom beam source, C_0 and C_{180} are channeltrons.

Symmetric top molecules such as CH_3I are good candidates for orientation because the dipole moment does not average to zero during the course of rotation. Unlike diatomic molecules (which rotate in a plane thereby causing the dipole moment to average to zero), symmetric top molecules rotate in an electric field like a child's top in a gravitational field: the symmetry axis precesses about the field and the dipole moment does not average to zero. In the collision-free environment of the molecular beam, *each* symmetric top molecule is therefore oriented with respect to a weak applied field, but since all orientations are present, the beam has no net orientation. To produce an *oriented* sample it is only necessary to remove the orientations that are not wanted, and this is accomplished by passing the beam through an inhomogeneous electric field in which the deflection of a molecule depends upon its orientation.

The energy interaction, $W = \boldsymbol{\mu} \cdot \mathbf{E} = -\mu_0 E\langle\cos\theta\rangle$, of a symmetric top molecule with an applied field is given by the first-order Stark effect [8], $W = -\mu_0 EMK/J(J+1)$, where μ_0 is the dipole moment, and J, K, and M are respectively quantum numbers for the total angular momentum, the component along the top axis, and the component along the field. Hyperfine interaction is neglected. Classically, $\langle\cos\theta\rangle \Rightarrow MK/J(J+1)$, where θ is the average angle between the symmetry axis and the electric field. In an inhomogeneous electric field, symmetric top molecules experience a force $\mathbf{F} = -\nabla W$ depending on the *sign* of $M \cdot K$ (or $\langle\cos\theta\rangle$), with each molecule to minimize its energy. *Any* inhomogeneous field will suffice in principle to separate the orientations, but it is useful experimentally to use a hexapole field because molecules with negative $\langle\cos\theta\rangle$ are *focused* by the field [9]. Molecules with negative $\langle\cos\theta\rangle$ can thus be spatially separated from those with positive $\langle\cos\theta\rangle$, and the hexapole field can serve as a state-selecting filter, rejecting molecules in states with positive values of $\langle\cos\theta\rangle$, and passing molecules in states with negative values of $\langle\cos\theta\rangle$. These molecules are oriented with respect to the local, non-uniform field inside the hexapole field. At the exit of the inhomogeneous field, an additional *uniform* electric field is imposed by parallel-plate electrodes. The E field thus gradually changes from the inhomogeneous field inside the hexapole to a uniform field in the collision centre. The field changes very slowly in comparison to the rotation of the molecule and the molecular rotation is quantized on the local field seen by the molecule. In the collision zone each molecule thus has a negative value of $\langle\cos\theta\rangle$, and true orientation is achieved. This is discussed in greater detail below.

An ideal hexapole field consists of six alternatively charged hyperbolic rods and the electrostatic potential inside this array is given by

$$V = V_0(r/r_L)^3 \cos 3\phi, \tag{6}$$

where r is the distance from the axis, r_L the axial distance to each electrode, V_0 the magnitude of the voltage on the rods, and ϕ is the polar angle. (Circular rods are usually used experimentally [1 (*d*)].) The radial force on a symmetric top molecule in such a field is independent of ϕ, and is given by

$$F_r = \mu\langle\cos\theta\rangle 6V_0 r/r_L^3. \tag{7}$$

For negative values of $\langle\cos\theta\rangle$, a molecule thus experiences a restoring force towards the axis, and the molecule can execute simple harmonic motion about the axis. Newton's equations predict that molecules entering the field with no radial component of velocity will be focused to a point on the axis when the voltage is

$$V_{\text{focus}} = \frac{\pi^2 v^2 m r_L^3}{24\mu L^2\langle -\cos\theta\rangle}. \tag{8}$$

If only a few rotational states are populated, $\langle\cos\theta\rangle$ assumes a few discrete values, and *if the exit aperture is small enough*, the hexapole field will transmit individual J, K, M states depending on the voltage selected.

Figure 7 shows the transmission of a CH_3Br beam calculated for two limiting exit apertures for our experimental conditions. ($T_{\text{translation}} = T_{\text{rot}} = 10$ K, $L = 1{\cdot}4$ M). At these temperatures, the most populated state is $|JK\rangle = |00\rangle$ which does not focus, but there is some population in the $|11\rangle$, $|21\rangle$ and $|31\rangle$ states, and these states are transmitted individually at appropriate voltages as shown. Molecules are thus actually focused by the hexapole field and, if only a few rotational states are populated, it is possible to select individual J, K, M states using appropriate combinations of applied voltage and beam apertures [10]. Focusing curves such as that in figure 7 have been measured experimentally, and reactive scattering has been observed for a few cases in which the beam is in a single quantum state [11]. (Unfortunately the intensity of such state-selected beams is extremely low; we have therefore chosen to study reactions with a distribution of states.)

For the focused molecules the rotationally averaged orientation is

$$\langle\cos\theta\rangle = M \cdot K/J(J+1), \tag{9}$$

where $\langle\cos\theta\rangle$ is the rotationally *averaged* cosine of the angle between the molecular dipole and the external field **E**. But at any instant, the probability of finding a molecule (in state $|JKM\rangle$) with a specific orientation with respect to the electric field is [12]

$$P_{JKM}(\rho)\,\mathrm{d}\rho = 4\pi^2|\psi_{JKM}|^2\,\mathrm{d}\rho, \tag{10}$$

where $\rho = \cos\theta$. The orientation distribution function P_{JKM} can be written as a short expansion of Legendre polynomials, and the probability distribution function is shown in figure 8 for several different $|JKM\rangle$†. Note that even for a single state, the molecule is not perfectly oriented ($\rho = -1$), and in fact the molecule has a small likelihood of being found with the 'wrong' orientation, $\rho > 0$. This is also predicted classically: a child's top will spin on the floor about its symmetry axis, which in turn precesses around the (gravitational) field. (On a finer scale, the angular momentum vector, $\mathbf{J}_s$, precesses about the field, and the symmetry axis nutates around $\mathbf{J}_s$.) The classical probability distribution function for a state analogous to $|212\rangle$ shows that the axis of the classical

† The states considered are pairs, $|J^{\pm}K^{\mp}M\rangle$, which are collectively referred to as $|JKM\rangle$.

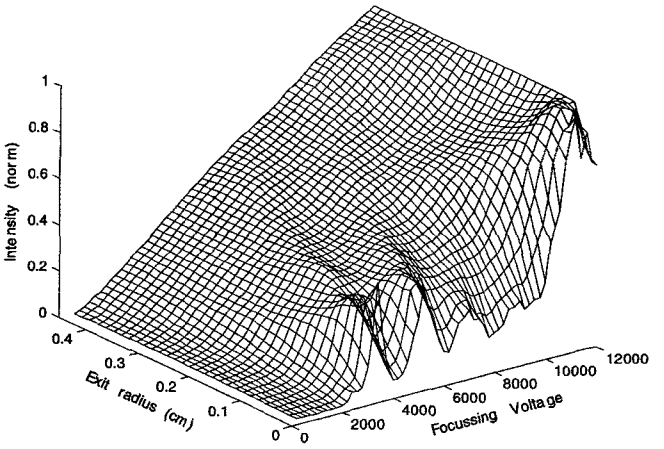

Figure 7. Calculated focusing curves (Intensity against V) for CH_3Br at 10 K for 1·4 M fields with different exit aperture radii. Rotational states for the smaller aperture are resolved; the larger aperture completely loses rotational structure but gains about twelvefold in intensity at 12 kV.

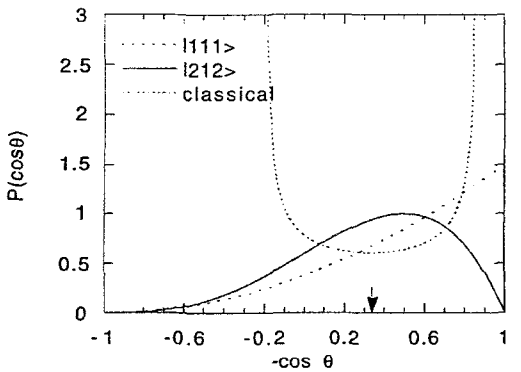

Figure 8. Quantum mechanical probability distribution functions for symmetric top molecules in the $|JKM\rangle = |111\rangle$ and $|212\rangle$ states. For comparison the classical distribution function corresponding to $|212\rangle$ is shown. The same average value of ρ (shown by the arrow to be $-0{\cdot}333$ for the $|212\rangle$ state) is obtained by averaging ρ over either the quantum distribution or the classical distribution, but the distributions are clearly different.

top also explores the wrong orientation. The quantum top can also point in directions where the classical top is not allowed.

In order to study reactive scattering in a variety of systems, we have greatly increased the flux of oriented molecules by enlarging the exit aperture of the hexapole field. Figure 7 shows how the focused intensity increases as the aperture is enlarged. Once the exit aperture becomes comparable to the deflection experienced by a molecule, the selectivity is diminished, and a given V_{focus} passes molecules in a variety of states. (Selectivity is also lost by increasing the population of higher J, K states, which occurs either at higher temperatures or for molecules such as CF_3Br which have more closely spaced rotational levels.) The hexapole thus acts mainly in a filter mode, passing molecules in states with negative values of $\langle\rho\rangle$ (where $\rho \equiv \cos\theta$) and an oriented sample is produced. The molecules which are passed populate a number of states and ray tracing techniques [13, 14] are used to calculate the probability $F_{JKM}(V_0)$ that molecules in states

$|JKM\rangle$ would be passed by the field. Thus, a collection of molecular states results, each state with a different orientation distribution. The overall distribution of orientations of molecules passed by the field, $P(\rho)$ is a sum over the distribution of individual states (similar to figure 8) weighted by the population of each state,

$$P(\rho) = A \sum_{J} \sum_{K=1}^{J} \sum_{M=1}^{J} P_{JKM}(\rho) f_{JK}(T) F_{JKM}(V_0), \tag{11}$$

where $f_{JK}(T)$ is the fraction of molecules in state J, K at temperature $T = T_{\text{rot}}$, $F_{JKM}(V_0)$ is the probability of transmission through the hexapole electric field, and $P_{JKM}(\rho)$, the probability distribution for state $|JKM\rangle$ which has been evaluated by Choi and Bernstein [12 (*b*)]. This composite probability distribution, calculated for the nominal focusing voltage of the $|212\rangle$ state, 5700 V, is shown in figure 9. For very small exit apertures, the resulting beam is essentially pure $|212\rangle$ (compare with figure 8) but as the aperture is enlarged, other states become included which emphasize $\rho \approx -1$. The distribution shown for the largest aperture is very robust; the calculated distribution is remarkably insensitive to the focusing voltage as well as to the rotational temperature assumed. (Our experiments show that, although the intensity increases with voltage, the focusing voltage has no major qualitative effect upon the orientation distribution.)

The probability distribution in figure 9 shows that the molecular sample obtained from the focusing field is oriented; an unoriented sample would have a uniform distribution over ρ. But even though the sample is *oriented*, the molecular axis has a non-zero probability of pointing in the 'wrong' direction ($\rho > 0$). This is easily understandable, because even the classical spinning top can be found pointing in the 'wrong' direction as a consequence of the nutation and precession of the top axis. (see Choi and Bernstein [12 (*b*)]). In addition, the quantum top can point in directions where the classical top is not allowed, which can easily be seen in figure 8 where the quantum distribution smoothly varies from $\rho = 1$ to $\rho = -1$ whereas the classical motion is confined to the range $0{\cdot}86 \geqslant -\rho \geqslant -0{\cdot}2$. The distribution shown in figure 9 is a weighted superposition of many curves similar (but more complex) to those of figure 8. Figure 10 compares calculated distributions for several molecules. As anticipated, the very prolate top CH_3Br (which, like a pencil, does not rotate easily about its symmetry axis), represents the least well oriented sample, and the oblate top CF_3H (which, like a bicycle wheel, rotates easily about its symmetry axis) the best. Even though each resulting distribution is quite broad, a large effect is observed on the reaction, as discussed below.

3.2. *Fast K atoms*

Beams of fast neutral potassium atoms are generated by charge exchange [15] of K^+ inside oven O. Atoms are surface ionized on a hot W filament located inside the oven, and the resulting K^+ ions are accelerated by voltage V to a grid ≈ 1 mm away. The K^+ ions drift ≈ 20 mm through a field-free low pressure ($\approx 0{\cdot}01$ mTorr) potassium gas in the same oven, and neutral K atoms with the same energy as the ions are produced by resonant charge exchange. The resulting beam contains some residual K^+ ions, fast neutral K atoms, and some thermal energy neutral K atoms. The residual ions are swept out of the beam by a deflecting field of $\approx 20\ \text{V cm}^{-1}$, and the thermal energy atoms do not interfere with these experiments because their energy is too low to produce ions. The results described here are due only to the fast neutrals.

The beam intensity is monitored by surface ionization on a cool W filament ($0{\cdot}13$ mm $\times$ 6 mm) located $0{\cdot}7$ m from the source. The ions formed by surface ionization

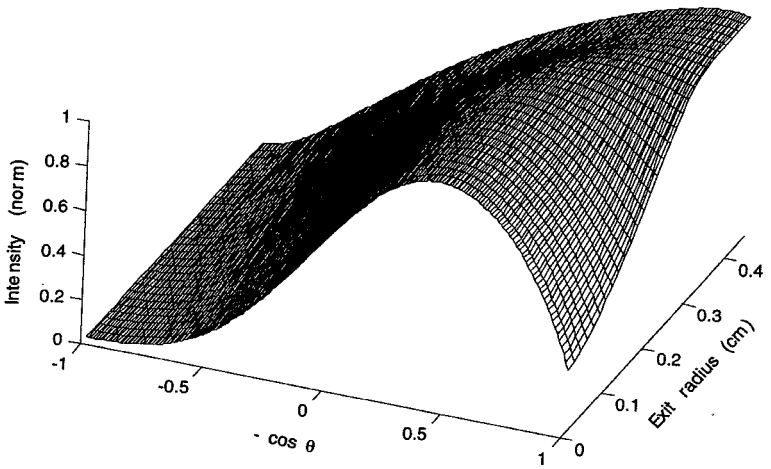

Figure 9. Calculated orientation distributions $P(\rho)$ for focusing voltage of 5700 V and different exit radii. Intensities are normalized to display structure for small radii. The intensity at maximum for the largest aperature is $\propto 12\times$ that of the intensity for the smallest aperature at its maximum.

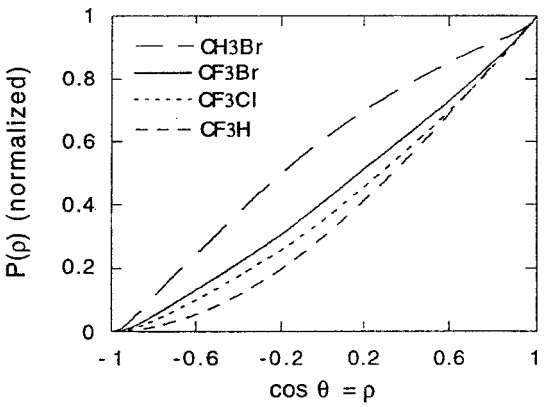

Figure 10. Distribution of orientations of molecules state selected by inhomogenous hexapole electric field.

on the wire are passed through a grid with a small (≈ 1 V) bias which discriminates against any ions resulting from surface ionization of thermal atoms, and the remaining ions are then detected by a crossed-field multiplier. Typical beam intensities are extremely low at energies of a few eV. The accelerating voltage in the source was used as the nominal laboratory energy in the early experiments [16]. Extensive time-of-flight measurements [17] of the fast beam energy have since shown that the actual energy was given to within the measuring error ($\approx \pm 2\%$) by the nominal energy. The energy spread is $\approx 4\%$.

3.3. *Beam intersection*

The beams intersect about 20 cm from the K oven inside a region of uniform field, U, generated by two plates parallel to the RX beam ≈ 5 cm apart (7·5 cm) which

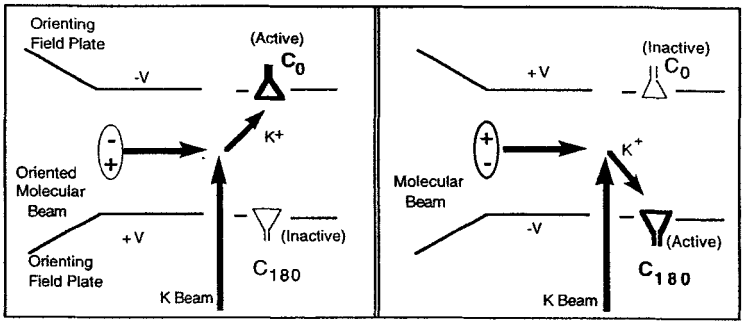

Figure 11. Polarities of the homogeneous orienting field and channeltrons used for the 0° and 180° configurations. The orientation of the polar molecule is indicated for each configuration.

approximately satisfies simultaneously the following two conditions: (1) in order for the molecules to be oriented they must be located in a region where the electric field direction is reasonably uniform and well-defined, and (2) in order for the ions to be detected, the nascent positive ions need to reach a channeltron.

The *direction* of the local field determines the *direction* of the molecular axes, and to provide uniform laboratory orientation a weak field (≈ 20 V cm^{-1}) is applied by the uniform field plates *U*. The molecules transmitted by the field are in high-energy states, so the positive end of the molecule points towards the positive field plate in region *U*. The laboratory orientation of the molecules is reversed by reversing the polarity of this uniform field. Holes are cut in the plates to pass the K atom beam, and to allow viewing of the intersection by two channeltron cones.

K^+ ions formed in the collision are detected by one or the other of the two channeltrons (C_{180} or C_0) arranged schematically as shown in figure 11. The voltage applied depended upon the orientation studied. The channeltron that peeked through whichever uniform plate was negatively biased was activated to count positive ions. The active cone was biased at -1200 (-1400 V) while its uniform plate was held at -50 V. The opposing plate and cone were held at $+50$ V, and both channeltron anodes were held at $+800$ V ($+300$ to $+700$ V, depending on gain requirements). For these operating conditions, the field at the intersection region is roughly determined by the parallel plates because it was observed that the channeltron counts decreased if the plates were biased much above 50 V, indicating that at higher voltages the ions would be collected only by the plates and not the channeltrons. Ions are less efficiently detected by channeltron C_{180}, apparently because the K^+ ions formed in the collision zone are initially moving away from C_{180}.

The orientation of the molecules is determined by the direction of the uniform electric field and may be reversed by reversing the polarity of the uniform field plates. As shown in figure 11, the positive end of the molecule is presented to the incoming K atom in the 0° configuration, and the ions counted by channeltron C_0. The negative end is presented in the 180° configuration and the ions counted by channeltron C_{180}. The experiments thus directly determine the polarity of the more reactive end; the chemical identity of the more reactive end must be deduced from electronegativities, dipole trends and the reactivity itself.

3.4. *Data acquisition*

The active channeltron is capacitively coupled to a quad scaler which counts signal pulses and pulses from an 8^6 Hz clock. Beam on-off signal differences at focusing voltage V, $S(V)_i = [S(V)_{on} - S(V)_{off}]_i$ are measured for each channeltron $i(i = 0$ or $180)$ and then corrected for the different multiplication efficiencies and ion collection efficiencies of each channeltron. The *relative* detection efficiency, $F(\varepsilon) = S(0)_{180}/S(0)_0$, is measured for each energy, interspersed with measurements of $S(V)$, using the small flux of randomly oriented molecules obtained when no voltage is applied to the six-pole field (0 kV). The *relative* signal due to the oriented molecules, $S'(V)$, is the (*HV* on)–(*HV* off) signal difference corrected for the multiplier efficiencies at beam energy ε: $S'(V)_{180} = S(V)_{180}$ and $S'(V)_0 = F \cdot S(V)_0$. For further details, see [7].

4. Results

4.1. *Raw signals*

In every case studied, the orientation of the molecule clearly affects the signal, and examples of this effect are shown in figure 12 for CH_3Br and CF_3Br. (We compare the methyl- and perfluoromethyl-halides because the polarity of the molecules is different: In CH_3X the X is usually negative, whereas the X in CF_3X is usually positive. This demonstrates that these data arise from a real molecular effect, and not from stray electric fields.) From the data in figure 12 we conclude that the *positive* end of CF_3Br is more reactive and the *negative* end of the CH_3Br is more reactive. The Br end of CH_3Br is assumed to be the negative end, and dipole moment trends and reactivity suggest that in CF_3Br the Br is the positive end, in nice analogy to CH_3 and CF_3I, where the I has been directly [18] and indirectly [19] established (by using oriented molecules) to be the positive end. Both molecules are thus more reactive on the Br end which we call the *heads* end (to emphasize the analogy with the heads/tails orientation of a coin). Similar conclusions are reached, with less refined data, in comparisons of the CF_3I/CH_3I and CF_3Cl/CH_3Cl systems. The data are thus not explicable by the electron simply jumping to the positive end of the dipole.

4.2. *Cross-section*

The energy dependence of the K beam intensity and the energy dependence of the reaction cross-section obscure the orientation dependence of the signals themselves. It is thus useful to remove the beam intensity variation by comparing the relative cross-sections $S'/I(K)$ for heads/tails orientation as shown in figure 13. The heads/tails difference is much more apparent and seems largest at low energies. The behaviour at high energies differs slightly from our early reports [16] because the monitor efficiency for fast K atoms was discovered to be slightly energy dependent. The space charge limited relationship, $I_K \propto E^{3/2}$, is used here to normalize the ion signals at different K beam energies, because the neutral intensity is expected to be proportional to $E^{3/2}$, as experimentally observed by Aten *et al.* [20] and roughly confirmed here.

4.3. *Steric effect*

The effect of orientation on the cross section is striking, but is still hidden by the variation of the cross-section with energy. The Steric factor, G, the signal difference normalized to the cross-section

$$G = (S'_{180} - S'_0)/(S'_{180} + S'_0) \tag{12}$$

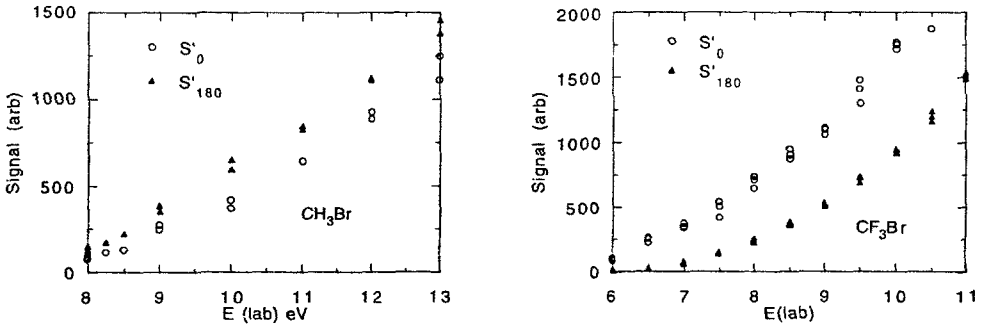

Figure 12. Relative signals for producing K^+ ions on collision with oriented CH_3Br and CF_3Br. The negative end of CH_3Br and the positive end of the CF_3Br are more reactive.

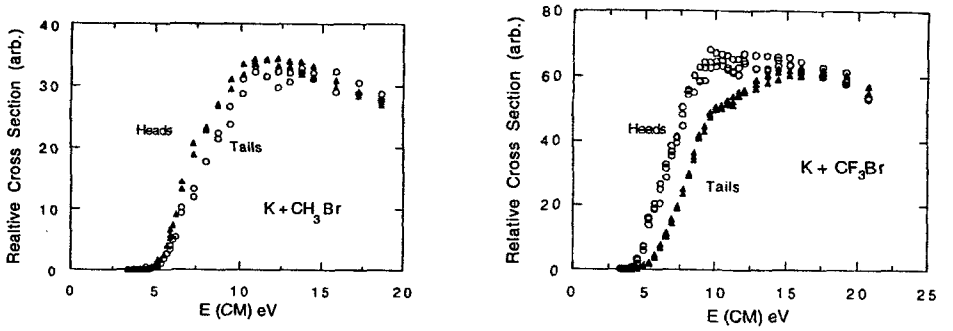

Figure 13. Relative cross-section (corrected ion signal/K beam intensity) for heads and tails orientations of CH_3 and CF_3Br.

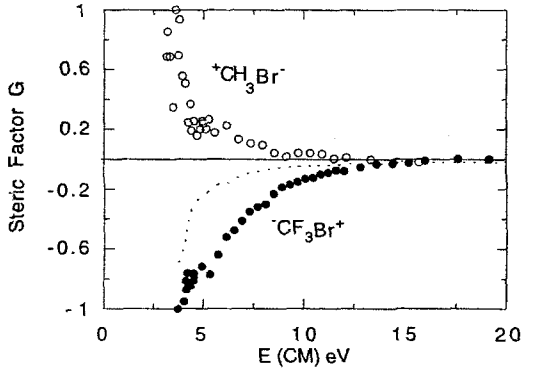

Figure 14. Steric factor G against centre-of-mass (CM) energy for CF_3Br and CH_3Br. Horizontal line is $G = 0$ (no steric effect) and dashed line is the negative of a smooth fit to the CH_3Br data plotted to compare the curvature of CH_3Br and CF_3Br.

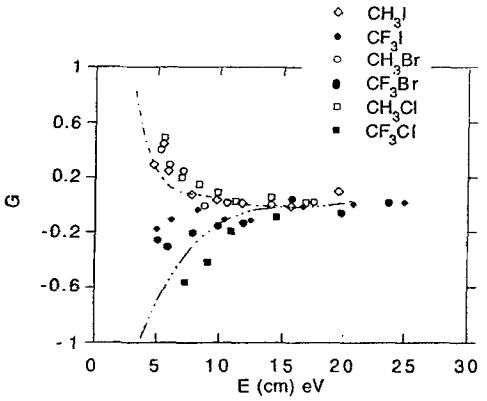

Figure 15. Comparison of experimental G values for CH_3X and CF_3X. The recent values of [7 (*b*)] are included as dashed lines, other data from [16].

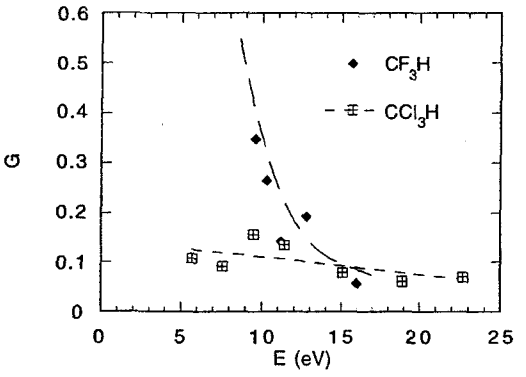

Figure 16. G values for CF_3H and CCl_3H [16]. Dashed line through CF_3H data represents the experimental values of [7 (*b*)].

emphasizes the salient features of the orientation itself, and is shown in figure 14 for the currently best-studied systems, CF_3Br and CH_3Br. The effect of orientation is striking: G must lie in the range $-1 \leqslant G \leqslant 1$, yet at low energy for both molecules G can clearly be extrapolated to ± 1. This means that at low energies one orientation is completely unreactive. At higher energies G tends to 0 and the orientation makes almost no difference. The difference in molecular polarity is immediately apparent, with the heads, or Br end being more reactive in either case. This difference persists throughout the CH_3X/CF_3X family, as shown in figure 15. Other types of systems, such as t-butyl X and CX_3H, display somewhat similar features, and are shown in figure 16 and [16].

4.4. *Threshold behaviour*

Extrapolation of G to low energies yields $|G| = 1$, at least for CF_3Br, CF_3Cl (not shown) and CH_3Br. This implies that at threshold one orientation is unreactive and is consistent with our early suspicion [16] that different orientations have different kinetic energy thresholds. This is indeed the case, as shown in figures (17–19).

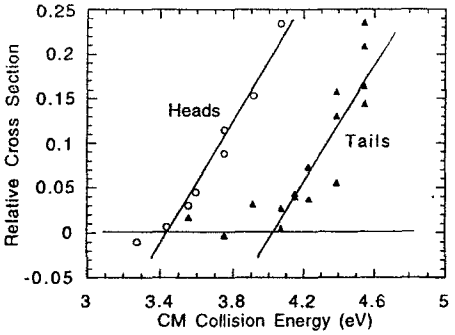

Figure 17. Relative cross-sections for heads and tails orientations for the K + CF_3Br reaction near threshold for ion production.

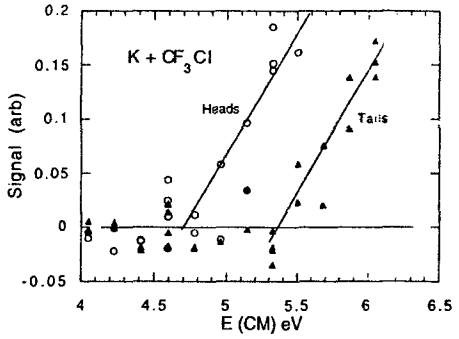

Figure 18. Threshold signals for oriented CF_3Cl.

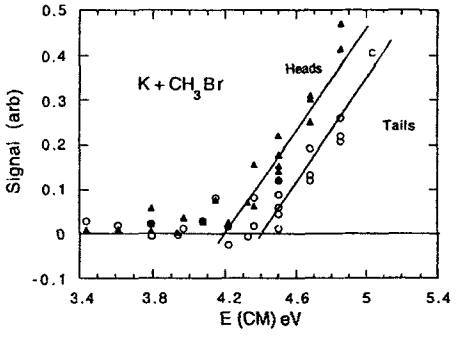

Figure 19. Threshold for oriented CH_3Br.

5. Discussion

5.1. *Caveat*

All chemical reactions begin at the reagents approach and end as the products separate. The system must traverse both the entrance channel and the exit channel. Our hope is that by specifying the reagent orientation in the entrance channel and monitoring the appearance of ions in the exit channel, that we may learn how orientation affects the transfer of an electron from one species to another. Strictly speaking, we cannot separate the electron transfer, presumed to occur in the entrance channel, from the process of the ions separating, which is the exit channel. Under certain circumstances, one or the other of these interactions may dominate. We have thus interpreted the data under certain assumptions, but what we *really* learn is how the entire process is affected by the initial molecular orientation, and conclusions regarding the electron jump must be regarded in this light.

5.2. *'Exit' channel interactions*

Angular distributions of the products of many chemical reactions bear a resemblance to the distributions obtained from photodissociation, suggesting that the products are formed in an impulsive event similar to photolysis [21]. It has been useful to compare experiments with a 'direct interaction with product repulsion' (DIPR) model. We have found this concept to be useful in interpreting the angular distributions of the neutral products of thermal energy collisions of oriented molecules. Early studies of the K + oriented CF_3I reaction suggested that the (neutral) KI product molecule was scattered in the direction in which the CF_3I figure axis was originally pointing [19]. The neutral KI molecule is found to be scattered backwards for K incident on the I end of the molecule and forwards for K incident on the CF_3 end. Cross-sections for the 'heads' and 'tails' orientations were roughly equal. Because the lowest unoccupied molecular orbital (LUMO) receiving the electron might be rather diffuse, we had originally assumed (mainly for simplicity) that the initial electron jump might be relatively unaffected by the orientation of the molecule, and further analysis indicates that the angular distribution of heads, tails and sideways oriented molecules is primarily described by the distribution of directions of the molecular axes [14]. These experimental results are semiquantitatively reproduced by the impulsive DIPR model sketched in figure 20 when the effect of the incoming K atom's momentum is included. Moreover, this model also accounts for the totally different angular distribution observed if the molecule is oriented sideways [22]. (It only partially accounts for the angular distribution observed for the analogous CF_3Br reaction [23], which inspired us to question whether the orientation affects the electron transfer.) It thus appears that the breakup of the molecular negative ion plays an important role in determining the angular distribution of the products, and may be important also in describing the higher energy ionization collisions.

The collisional ionization experiments of unoriented molecules mentioned in section 2 provide the key to understanding the exit channel interactions for oriented molecules: there must be two ionic/covalent surface crossings, one as the particles approach, and the second as they recede, qualitatively sketched in figure 4. In a limiting case of 'bond stretching', the molecular ion might be in the process of dissociating by the time the second crossing is encountered. This is shown very schematically in figure 21, where the covalent K + RX surface crosses the ionic $K^+ + RX^-$ surface at r_{c1}. This crossing distance $r_{c1} = e^2/\Delta E_0$ is calculated from ionization potentials and

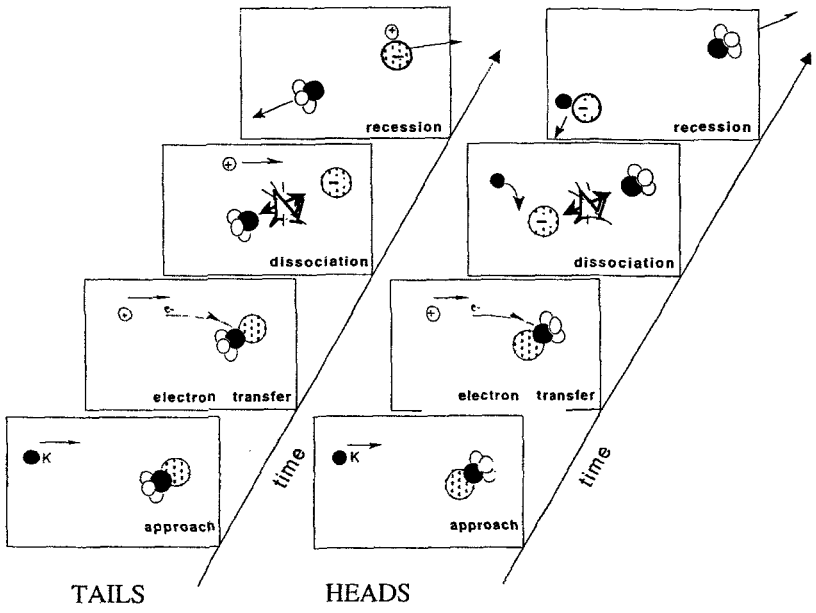

Figure 20. Schematic mechanism for impulsive reaction of thermal energy reaction of K with oriented CF_3I. The electron is assumed to be transferred at large distance to the molecule irrespective of orientation. The molecular ion is formed in a repulsive state which promptly dissociates, ejecting the I^- ion in the direction of the molecular axis. The K^+ is dragged off by the departing I^-, resulting in backward scattering for heads orientation and forward scattering for tails as observed.

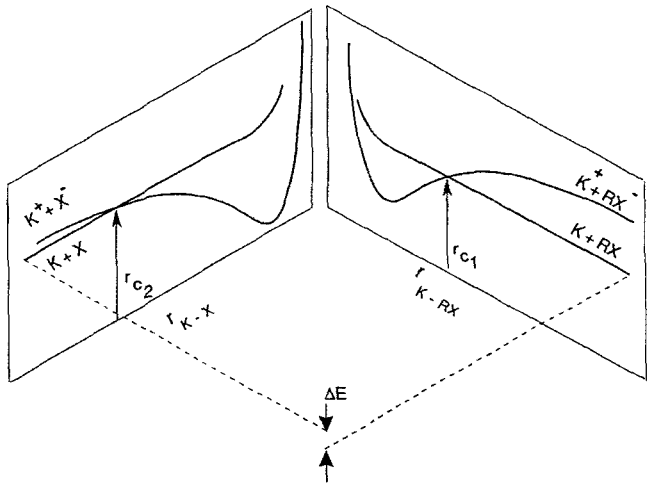

Figure 21. Highly schematic one-dimensional representation of electron jump in a dissociating molecular system. Neutral K and *RX* approach on a covalent surface on the right, crossing the ionic surface at r_{c1} which is at sufficiently short range for the surfaces to be separated and for the system to traverse the crossing adiabatically. (The electron jumps.) After electron transfer, the negative ion can undergo a dissociation (migrating to the left panel), and the system evolves along another surface to give fragments K^+, X^-, and *R*. These undergo a crossing r_{c2} at larger distances with neutral fragments K, *X* and *R*, where the surfaces are not well separated. The system is more likely to traverse this crossing *diabatically*, and the fragments will separate as charged species.

electron affinities to be ≈ 4 Å, and $H_{IC} \approx 300$ meV. At the nominal collision speeds used in these experiments, $v_r \approx 5{\cdot}6$ km s^{-1} (56 Å (ps)$^{-1}$) for CH_3I at 5 eV, the Landau–Zener relation, equation (2), predicts that $P_d \approx 0$, and the first crossing will be completely adiabatic: the electron will jump to the molecule. The electron is expected to occupy an antibonding C–X σ^* orbital and the molecular ions produced, CF_3X^- and CH_3X^- are expected to dissociate promptly along yet another surface (in another dimension on the left panel), indicated as $K^+ + R + X^-$. This surface will intersect the $K + R + X$ covalent surface at a much larger distance, r_{c2}. Since H_{IC} decreases exponentially with distance [5], this crossing is less avoided, and the system is more likely to traverse this crossing diabatically with the electron remaining on the X^- ion.

At energies a few volts above threshold, the CH_3I, CF_3I, CH_3Br and CF_3Br molecules undergo dissociative electron attachment [24] and in collisional ionization give X^- ions in $\approx 98\%$ yield [25]. The scenario suggested above (the electron jumping at the first crossing and the molecular ion dissociating before the second crossing is encountered) is thus very likely to occur. If the molecule were to remain unchanged upon the addition of the electron, the second crossing would be exactly equivalent to the first and would again be traversed completely adiabatically. The electron would be smoothly transferred back to the K^+, the products would separate on the covalent surface, *no* ions would be produced, and there would be no dependence on orientation. If, on the other hand, the molecular ion were to decompose explosively, the second curve crossing would be an asymptotic crossing between the emerging X^- ion and the incident K^+. This second crossing occurs at large R where $H_{IC} \approx 0$. The LZ relation then predicts that the second crossing would be completely diabatic, the electron would stay on the X^- ion and the products would separate on the ionic surface. In this latter limiting case every collision would lead to ionization and the orientation would not be important.

The behaviour observed is clearly intermediate between these two limits: ions are produced and the orientation is important. The existence of an orientation effect shows that every collision does not lead to ionization. As discussed above, we expect the electron to be transferred adiabatically at the first crossing. But at the second crossing the K^+ ion must be encountering something intermediate between a bound CF_3Br^- molecular ion and a free Br^- atomic ion. It must encounter a species in the act of breaking apart, and we can use the experimental orientation data to extract some information about this species.

We assume the first crossing is completely adiabatic, and that the probability of the K escaping as K^+ is the probability that the second curve crossing is traversed diabatically,

$$P_d = \exp(-\kappa/v). \tag{13}$$

Note that this is sensitive to the *relative speed* of ions at the crossing, which as shown in figure 22, is different for the heads and tails orientation. Making the zeroth-order approximation that κ is independent of orientation, then the probability of forming an ion in the heads or tails orientation is

$$P_\xi = P_d = \exp(-\kappa/v\xi), \tag{14}$$

where ξ refers to either heads or tails. The heads/tails ratio then becomes

$$R = P_h/P_t = \exp(-\kappa/v_h + \kappa/v_t) = \exp(-\kappa\Delta v/v^2). \tag{15}$$

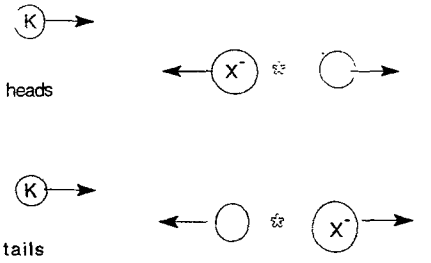

Figure 22. Schematic illustration of velocity components as molecular ion dissociates in heads and tails orientations. In the heads orientation, the nascent ions collide head on with a higher relative velocity than in the tails orientation, where one ion must catch up with the other.

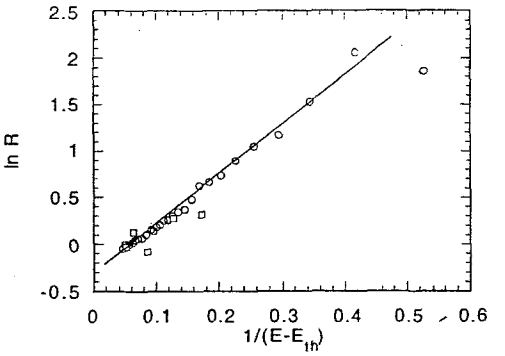

Figure 23. $\ln R$ against $1/E - E_{th}$ for CF_3Br. Circles from [7 (*b*)] and squares from [16]. Deviations from line are accentuated for low E.

where

$$\Delta v = v_l - v_h \text{ and } v^2 = v_h v_l \approx 2E'/\mu. \tag{16}$$

A plot of $\ln R$ against $1/E'$ is thus expected to be linear, where E' is the final translational energy, $E < E - E_{th}$. This is shown for CF_3Br in figure 23. For energies a few volts above threshold, the orientation effect is well described by equation (2). (At high energies the first crossing may become diabatic thereby invalidating the assumption made in equation (13). Uncertainty in E_{th} and fluctuations in the very low signals probably accounts for deviations near E_{th}.)

Thus, the impulsive model described in figure 22 accounts nicely for energy dependence of the orientation effect. In the exit channel the ions are trying to get away from one another, and this is easiest if they are travelling in opposite directions, which occurs in the heads orientation. The second ionic/covalent surface crossing occurs between species in the act of reacting, and an experimental value for κ at this second crossing can be obtained from the slope of a plot such as figure 23. Semi-empirical estimates for H_{IC} have been used to obtain rough values of r_2, and suggest that r_2 may be an Å or two larger than r_1, consistent with the notion that the crossing is between at K^+ ion and a species in the act of coming apart [16].

Thus, many aspects of the collisional ionization experiments can also be described by the impulsive DIPR mechanism, provided the very strong interaction between the ions in the exit channel is recognized. This is qualitatively depicted in figure 24, which

differs from figure 23 in two major respects: (*a*) the incoming K atom is faster, and (*b*) ions are detected, not neutrals. As shown, the approach, the electron transfer, and the dissociation steps are similar to those at lower energy, and the negative atomic ion is again ejected in the direction of the molecular axis. The K atom is now much faster and the K^+ ion is more likely to continue in the forward direction. If the X^- ion is ejected antiparallel to the incoming K^+, the ions have less time to interact, and in the 'heads' orientation the K^+ is more likely to escape the Coulomb attraction of the X^- and be detected as an ion. Similarly, in the tails orientation the X^- travels parallel to the K^+, the ions are more likely to either recombine or to neutralize one another, and fewer K^+ ions escape the Coulomb attraction.

Independent support for these conclusions regarding the orientation effects in the exit channel is provided by the experiments of Kalamarides *et al.* [26]. Reaction of K atoms in high Rydberg states with CF_3I, $K^{**} + CF_3I \rightarrow K^+ + I^- + CF_3$ was studied by passing a beam of K** through a scattering gas containing low pressure CF_3I, and measuring the angular distribution of the resulting I^- ions with a microchannel plate and position sensitive detector.

For large principal quantum numbers, $n \approx 26$, the Rydberg electron is essentially free of the core and behaves as a free electron. The CF_3I was a gas and all orientations of the molecules were equally likely, so CF_3I^- ions were expected to be formed in all orientations by attachment of the 'free' electron. Dissociation of CF_3I^- would eject I^- along the randomly oriented molecular axes, and the I^- ions were expected to be distributed isotropically, and this was confirmed by experiment. However, as n decreased to 9, the angular distribution became anisotropic, with fewer I^- moving in the direction of the initial K**. The electron is more tightly bound for $n = 9$, and is more comparable to those of this study ($n = 4$): the Rydberg electron in this case is not free, but carries with it the positively charged core. Kalamarides *et al.* thus observed that fewer I^- ions were scattered in the forward direction and concluded that the diminution of I^- in the forward direction was due to a greater likelihood of charge neutralization if I^- and K^+ were travelling in the same direction as concluded from the oriented molecule experiments and shown in figure 24.

5.3. *Entrance channel: the electron transfer*

The Landau–Zener theory is comparatively successful in explaining the overall behaviour of the reactions of oriented molecules at thermal energies where neutral products are formed and at elevated energies where the transient ions have enough energy to separate. This is, in a sense, frustratingly successful, because there seems to be no room to accommodate an orientation-dependent electron transfer, which chemical intuition suggests must be operative.

The role of the electron transfer in the post-threshold behaviour discussed above is perhaps overshadowed by the strong Coulomb forces in the exit channel. Orientation dependent exit channel interactions are possible when three or more species are produced in the collision as shown in figure 22, and as discussed above, this is likely the case for several of the molecules studied. But if the collision energy is sufficiently low, decomposition of the molecular negative ion may not be allowed. If only two particles are formed, a positive ion and a negative ion, conservation of momentum requires that they must recede with antiparallel velocities regardless of the orientation. The strong, orientation-dependent forces in the exit channel suggested in figure 22 are thus not present, and any orientation effect may be due to the electron transfer in the entrance channel.

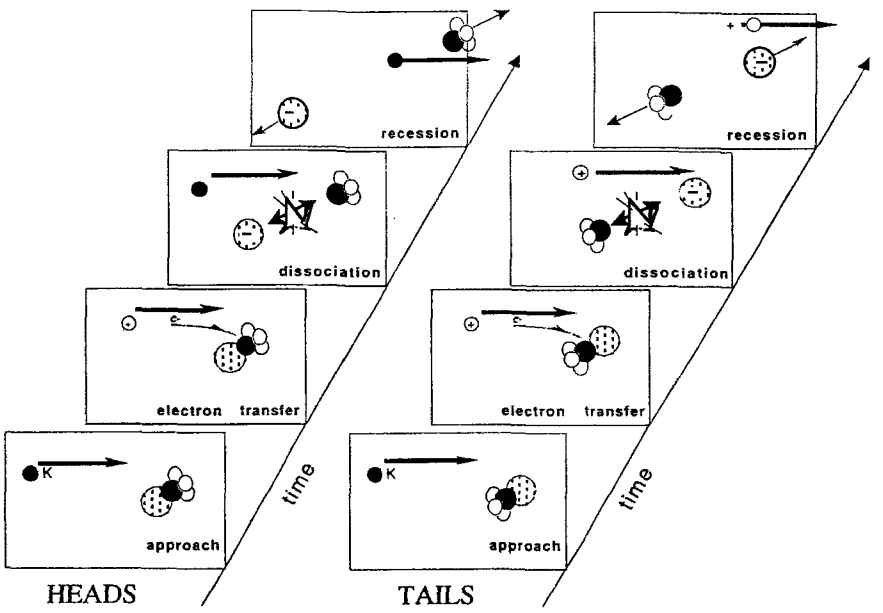

Figure 24. Schematic mechanism for impulsive reaction of high energy K with oriented CR_3X. Similar to figure 20, but the higher speed K^+ ion is much less perturbed by the X^-. Parallel trajectories (in the tails orientation) allow for longer contact time resulting in some neutralization and a concomitant reduction in ion signal.

The different threshold behaviour for head and tails orientations shown in figures 17–19 shows that that at very low energies reaction is restricted to *only one end* of the molecule. We observe directly that there is no reaction for attack in the unfavoured orientation. The different thresholds for attack at different 'ends' of these molecules requires the final state of the system, at the respective thresholds, to be somehow different for attack at the opposite ends of molecule. For CF_3Br we believe that different *products* may be formed, depending on the end attacked, but the same species in different internal (say vibrational) states could also be a possibility [27].

In these experiments there are two likely low energy reaction channels:

$$K + CX_3Y \rightarrow K^+ + Y^- + CX_3 \tag{17}$$

$$\rightarrow K^+ + CX_3Y^- \tag{18}$$

which we are not yet able to differentiate because only the K^+ positive ion was detected. (KY salt molecules might also be formed but since only charged particles are detected, the neutrals are not observed.) At energies a few volts above threshold, the fragmentation reaction (17) accounts for $\approx 95\%$ of the products [25] and the early experiments were interpreted on the basis of reaction (17). At sufficiently low energies, however, the parent ion may not have enough energy to fragment and reaction (18) can be observed.

The negative ions formed in collisions of Na atoms with unoriented CF_3Br have been directly observed by Compton, Reinhardt and Cooper [25]. They observed the parent ion, CF_3Br^- and determined the vertical electron affinity, EA_v, to be $0{\cdot}91 \pm 0{\cdot}2$ eV. From their data the threshold for electron transfer to CF_3Br to give the parent ion (18) is 3·43 eV and the threshold for fragmentation (17) to give Br^- is 3·97 eV.

These threshold energies for formation of the parent ion, CF_3Br^-, and for fragmentation into CF_3 and Br^- agree closely with the apparent thresholds obtained for the oriented molecules 3·4 eV and 4·0 eV. (Since the threshold laws are not known, we have determined *apparent* thresholds by linear extrapolation of the data shown in figures 17–19. The thresholds differences are expected to be significant because the cross-sections for heads and tails orientations are similar over a large energy range [17].) We thus conclude that, at the lower (heads) thresholds, parent CF_3Br^- is produced, and it is produced by attack at the Br end of the molecule. In the energy range 3·4–4·0 eV, reaction occurs *exclusively* at the heads (Br) end of the molecule producing only two particles, K^+ and CF_3Br^-, which must leave the collision travelling in opposite directions to conserve momentum. The strongly orientation-dependent three-body exit channel interactions, which were adequate to explain the high energy (≈ 10 eV) orientation behaviour, are therefore absent. Effects of orientation between 3·4 and 4·0 eV must arise mostly from the electron transfer in the entrance channel, and we conclude that for energies near threshold the electron is transferred preferentially to the Br end of the molecule.

At the higher (tails) threshold, tail end attack results in fragmentation and produces Br^- fragments. Formation of the parent negative molecular ion by tails attack is apparently prevented by some barrier which can be overcome with $\approx 0{\cdot}5$ eV of translational energy. But the CF_3Br^- molecular ion is too weakly bound to accommodate this much energy, and the negative molecular ion breaks up according to reaction (17). (Above the tails threshold, heads attack may also produce Br^- fragments because enough energy would likely be deposited in the parent ion to cause it to break apart, and above about 5 eV, Br^- is the dominant negative ion.)

For the other molecules studied, less is known about the negative ions formed and their thresholds. It is, of course, tempting to speculate that different products are being formed for different orientations in a manner analogous to that for CF_3Br and for the electron bombardment experiments. For CF_3Cl the parent ion has been observed [28], and figure 18 shows a clear *difference* between heads and tails thresholds of $\approx 0{\cdot}6$ eV. Again, the Cl end is more reactive and at low energies only Cl-end attack produces ions. However, the apparent threshold is in poorer agreement with that calculated, possibly a result of the extrapolation of our weaker signals because the reaction cross-section is smaller than that for CF_3Br.

The parent CH_3Br ion has not been observed in previous studies [25, 29]. Nevertheless, figure 19 shows that only one end of the molecule, the Br end, is reactive at energies near threshold. The difference in thresholds is $\approx 0{\cdot}2$ eV, and the tails threshold is in rough agreement with the calculated threshold to produce Br^- and with the observations of Compton *et al.* for the formation of Br^-. If the analogy with CF_3Br is pursued, these data indicate that the parent ion is bound only by $\approx 0{\cdot}2$ eV ($\pm \approx 0{\cdot}2$ eV), suggesting that the parent may be so fragile that it might not be observed.

These data thus suggest that different products are formed by attack at different ends of the molecule, which are manifested here by different energetic thresholds for the two orientations. In similar experiments, Aitken, Blunt and Harland [30] have recently discovered that electron bombardment of oriented CH_3Cl produces more parent CH_3Cl^+ for attack at the CH_3 end of the molecule, but that the formation of CH_3^+ seems to be independent of orientation.

The electron probably jumps to an antibonding $p\sigma^*$ orbital composed largely of p orbitals from carbon and bromine [28], which is expected to be more accessible from

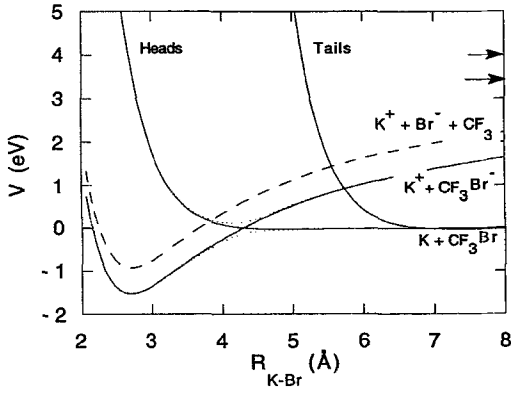

Figure 25. Approximate (one-dimensional) ionic and covalent diabatic potentials adapted from [31] for CF_3Br. Solid and dashed ionic curves are Rittner-type potentials for parent and fragment ions respectively, and heads and tails are covalent curves. The ionic asymptotes are denoted by arrows. The crossings are avoided; dotted curves for the 'crossing' near 4·3 Å are the adiabatic curves resulting from configuration interaction [5] between the diabatic ionic and covalent curves. (Adiabatic curves for the other crossings are omitted for simplicity.)

the Br end of the molecule. The threshold results show that transfer through the CF_3 end is apparently impeded by a barrier of about 0·6 eV (14 kcal mole^{-1}), which can be overcome by increasing the collision energy, resulting in fragmentation of the anion. This is qualitatively illustrated by the potential curves in figure 25 where the covalent potential for tails approach includes an extra repulsion term to account for the CF_3 group interposed between the K and Br. This extra repulsion forces the tails orientation crossing to be at larger distances (and higher energies) where electron transfer is much less likely because the orbital overlap is less. The interaction between the ionic and covalent configurations falls exponentially with distance [5], and at a given collision energy, the likelihood of an adiabatic crossing (electron jump) is greatly decreased, which mostly accounts for the lack of ions formed in the tails orientation. The higher energy of the crossing provides some rationale for the barrier to tails attack. (This description and figure 25 are highly simplified because additional dimensions, such as the C–Br distance, must be considered to explain salt formation as well as the fragmentation observed at higher energy.)

The conclusion that electron transfer is localized is likely to apply to other systems, even at lower energies. As the energy is decreased towards thermal energy, the electron is more likely to 'jump' although *the electron will jump back* if the energy is below threshold, which is likely the case for tails attack below tails threshold. Salt formation (exoergic by $\approx$ 20 kcal mol^{-1}) and ion production compete with one another above the ion threshold, and it is reasonable to conclude that these processes share the same entrance channel. The preference for the Br end is thus expected to extend to lower energies, and indeed in an earlier study of K + CF_3Br at thermal energies [23], we found that the neutral salt, KBr, was more likely to be formed by Br-end attack. (While overall production of K^+ is greater at all energies for 'heads' attack, we are as yet unable to assess the relative importance of 'heads' against 'tails' attack on the Br^- channel at the onset of Br^- formation.)

5.4. *Reaction models*

Reaction probability is clearly dependent upon the orientation, as shown in the previous section. Because G can be extrapolated to ± 1 at low energies, it is clear that some orientations must be completely unreactive. As discussed in section 3, the orientation is not perfect, but instead the distribution of orientations, such as predicted in figures 9 and 10 shows that the molecular axes are likely to be found over the entire range of angles, from $\rho = -1$ (perfectly oriented) to $\rho = +1$ (oppositely oriented), although the distribution is skewed towards $\rho = -1$. Comparison of 'heads' and 'tails' thus always mixes a little of one orientation into the other, and the reactivity is expected to depend even more sensitively on orientation than shown by the experiments.

In order to estimate how the reaction probability varies with angle of attack, we use a very simple step function model qualitatively shown in figures 26 and 27. (Many more elaborate models could be adopted but the single experimental value of G at each energy does not provide a basis for distinguishing one from another.) The orientation distribution function for CF_3Br of figure 10 is replotted against $\cos\chi$, where χ is the angle between the molecular axis and the relative velocity of the incoming atom. (The distribution of molecular axes with respect to the orienting field remains as shown in figure 10, but in the 'heads' orientation $\mathbf{E}$ and $\mathbf{v}_r$ are parallel, and in the 'tails' orientation, $\mathbf{E}$ and $\mathbf{v}_r$ are anti-parallel.) The reaction probability, P, is assumed to be given by

$$\left.\begin{aligned} &P(\cos\chi) = 1, \quad \cos\chi_c \geqslant \cos\chi \geqslant -1, \\ &P(\cos\chi) = 0, \quad \text{otherwise.} \end{aligned}\right\} \tag{19}$$

The fraction reacting in each orientation is thus the convolution of the rectangular reactivity function $P(\cos\chi)$ with the orientation distribution $P(\cos\chi)$. By calculating G for various χ_c and equating the experimental G with the calculated G, we are able to extract χ_c for each energy. These results are shown in figure 28.

Figure 28 shows that at energies near threshold, reactivity is restricted to a very narrow cone about perfect 'heads' orientation. This cone opens up as the energy increases, and at about 7 eV for CF_3Br the reactive cone has expanded to encompass the entire Br hemisphere. The reactive cone encompasses the entire molecule (i.e. any orientation is reactive) at energies greater than about 20 eV for CF_3Br. For CF_3X, (X = Br or Cl) the opening of the reactive cone extends over 3–4 eV, but the 'turn-on' of reactivity for CH_3Br is much more precipitous, occurring over $\approx$ 1 eV, which can also be seen in the steric factor G in figure 14.

The main conclusions here is that χ_0 is very small near threshold and becomes larger as the energy is increased. These are restatements of the experimental data and should not be dependent upon the reaction model. The variation of χ_0 with energy obviously show that the steric effect varies with energy, and the amount of 'steric hindrance' in a reaction (as well as the 'steric factor') will also depend on energy, and should not be considered as a constant.

The energy dependence of the cut-off angle is roughly given by an Arrhenius-type of dependence,

$$\chi_0 \propto \exp\left(\frac{-B}{E - E_{th}}\right), \tag{20}$$

where E_{th} is the threshold energy and B is a parameter characterizing the decay, normally interpreted as the height of some potential barrier. Figure 29 shows a plot of $\ln\chi_0$ against

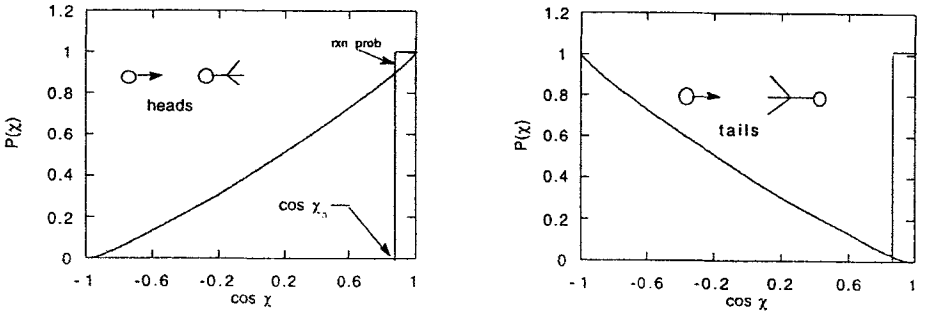

Figure 26. Distribution of molecular axes seen by incoming K atom for CF_3Br in the heads and tails orientations. These distributions are the quantum states for figure 10 referred to the relative velocity of the incoming atom. The rectangle on the right of each plot represents a step function model of the reaction probability P, which is one for the direct heads attack and remains one to some cut-off angle, χ_0 and is zero beyond that angle.

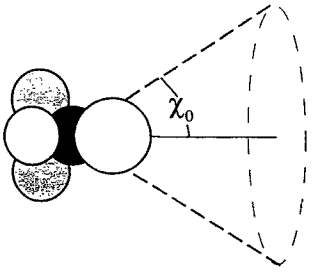

Figure 27. Schematic view of the reaction cone. The simple step-function model illustrated in figure 26 suggests that atoms with initial velocities lying within the cone of half angle χ_0 would react with unit probability, and velocities lying outside would not react.

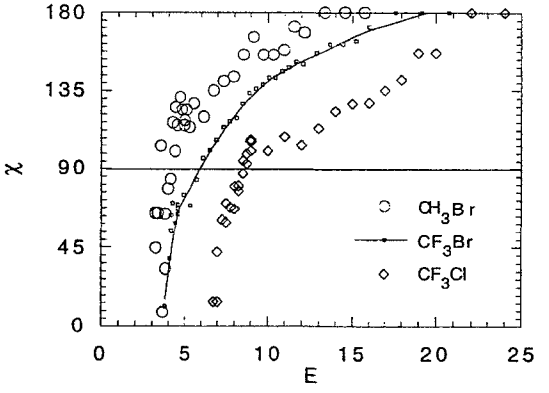

Figure 28. Cut-off angles for step function model of reactivity shown in figure 27. In order to react atoms must attack with angle $\leq \chi_0$ where χ is measured from the halogen end of the molecule. For points lying below $\chi = 90$, reaction does not occur for attack at the CF_3 or CH_3 hemisphere.

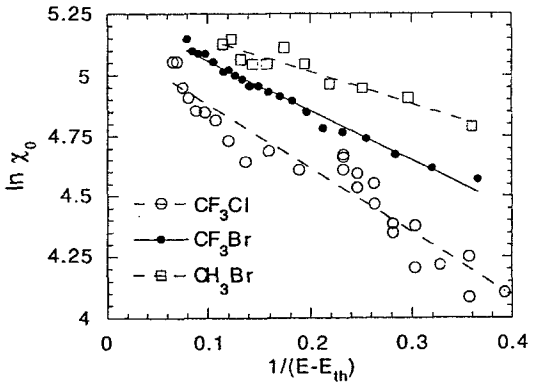

Figure 29. Energy dependence of cut-off angle, plotted as ln χ_0 against $1/(E\text{-}E_{th})$. Lines are least square fits to the data. Uncertainties in E_{th} cause data points at lower energies to deviate from these lines.

$1/(E - E_{th})$ for CF_3Br, CF_3Cl and CH_3Br, together with least square fits to the points. Values of B derived from these fits are, respectively, 2·05, 2·64, and 1·31 eV. Points near threshold were excluded from these determinations because they are less reliable and also more likely to include contributions from very low-energy channels such as those in which the parent ion is formed. These barrier values suggest that the hindering effect of the radical is the greatest for CF_3Cl, and the least for CH_3Br, and probably indicate the hindering effect of the $R(CF_3$ or $CH_3)$ group on reaction to form Br^- or Cl. These more detailed questions must be deferred pending the identification of single product channels.

Earlier electron spin resonance (ESR) studies suggest that the unpaired electron in CF_3X^- or CH_3X^- ($X = Cl, Br, I$) resides in an $p\sigma^*$ anti-bonding orbital composed largely of the p orbitals of carbon and X, the unique halogen [19]. Our results suggest that the X end of the molecule is more accessible for the electron transfer, and transfer through the CF_3 or CH_3 end is apparently impeded by a potential barrier. Using CF_3Br as an example, this barrier is $\approx 0{\cdot}6$ eV, and can be overcome by increasing the collision energy which then results in the fragmentation of the energized CF_3Br^- molecular ion.

6. Summary

Ions are formed in electron transfer collisions between beams of neutral K atoms and beams of *oriented* target molecules. In every case studied so far, the orientation of the target molecule greatly affects the reactivity, consistent with 'chemical intuition'. The electron is not, however, simply transferred to the positive end of the molecule, because in the methyl halides the negative end is more reactive.

At energies a few eV above threshold where molecular negative ions might fragment, the dynamics seem to be dominated by the ions getting away from one another. More than two particles can form, and the initial molecular orientation can be manifested in the exit channel as ions travelling with parallel or anti-parallel velocities. Ions with anti-parallel velocities are most likely to survive as ions, consistent with observation.

At low energies several molecules exhibit different thresholds for different orientations. There is consequently an energy region where no reaction occurs at the 'wrong' end of the molecule. A simple model averaged over the experimental

orientations suggests that reaction at low energies requires virtually collinear attack, and that this requirement is relaxed at the energy is increased.

Gratefully acknowledgment is made to the Robert A. Welch Foundation and to the Donors of the Petroleum Research Fund, administered by the American Chemical Society, for financial support of this research. This MS was begun during a US-New Zealand Cooperative Research program sponsored by the NSF, and I gratefully acknowledge this support as well as the hospitality of the University of Canterbury during my visit there.

References

[1] For reviews see (*a*) BROOKS, P. R., 1976, *Science*, **193,** 11; (*b*) BERNSTEIN, R. B., HERSCHBACH, D. R., LEVINE, R. D., 1987, *J. phys. Chem.*, **91,** 5365; (*c*) HARREN, F., PARKER, D. H., and STOLTE, S., 1991, *Comments At. Molec. Phys.*, **26,** 109; (*d*) PARKER, D. H., and BERNSTEIN, R. B., 1989, *Ann. Rev. Phys. Chem.*, **40,** 561; (*e*) STOLTE, S., 1988, *Atomic and Molecular Beam Methods*, Vol. 1., edited by G. Scoles (Oxford University Press), pp. 631–652.

[2] See (*a*) LOESCH, H. J., and REMSCHEID, A., 1990, *J. chem. Phys.*, **93,** 4779; (*b*) LOESCH, H. J., and REMSCHEID, A., 1991, *J. phys. Chem.*, **95,** 8194; (*c*) LOESCH, H. J., and MÖLLER, J., 1992, *J. chem. Phys.*, **97,** 9016; (*d*) FRIEDRICH, B., and HERSCHBACH, D. R., 1991, *Z. Phys.* D, **18,** 153, (*e*) SLENCZKA, A., FRIEDRICH, B., and HERSCHBACH, D., 1994, *Phys. Rev. Lett.*, **72,** 1806.

[3] For reviews of collisional ionization, see (*a*) KLEYN, A. W., LOS, J., and GISLASON, E. A., 1982, *Phys. Rep.*, **90,** 1; (*b*) LACMANN, K., 1980, *Potential Energy Surfaces*, edited by K. P. Lawley (New York: Wiley), p. 513; (*c*) BAEDE, A. P. M., 1975, *Adv. Chem. Phys.*, **30,** 463; (*d*) LOS, J., and KLEYN, A. W., 1979, *Alkali Halide Vapors* edited by P. Davidovits and D. L. McFadden), (New York: Academic), p. 279.

[4] BERRY, R. S., 1957, *J. chem. Phys.*, **27,** 1288.

[5] GRICE, R., and HERSCHBACH, D. R., 1974, *Molec. Phys.*, **27,** 159.

[6] KLEYN, A. W., KHROMOV, V. N., and LOS, J., 1980, *J. chem. Phys.*, **72,** 5282.

[7] (*a*) CARMAN, JR., H., 1986, PhD Thesis, Rice University; (*b*) XING, G., 1993, PhD Thesis, Rice University.

[8] TOWNES, C. H., and SCHAWLOW, A. L., 1975, *Microwave Spectroscopy* (New York: Dover).

[9] (*a*) BENNEWITZ, H. G., PAUL, W., and SCHLIER, CH., 1955; *Z. Phys.*, **141,** 6; (*b*) KRAMER, K. H., and BERNSTEIN, R. B., 1965, *J. chem. Phys.*, **42,** 767; (*c*) BROOKS, P. R., JONES, E. M., and SMITH, K., *Ibid.*, 1969, **51,** 3073.

[10] (*a*) GANDHI, S. R., XU, Q.-X., CURTISS, T. J., and BERNSTEIN, R. B., 1987, *J. phys. Chem.*, **91,** 5437; (*b*) KASAI, T., FUKAWA, T., MATSUNAMI, T., CHE, D.-C., OHASHI, K., FUKUNISHI, Y., OHOYAMA, H., and KUWATA, K., 1993, *Rev. scient. Instrum.*, **64,** 1150.

[11] JANSSEN, M. H. M., PARKER, D. H., and STOLTE, S., 1991, *J. phys. Chem.*, **95,** 8142.

[12] (*a*) STOLTE, S., 1982, *Ber. Bunsenges, phys. Chem.*, **86,** 413; (*b*) CHOI, S. E., and BERNSTEIN, R. B., 1986, *J. chem. Phys.*, **85,** 150.

[13] BROOKS, P. R., JONES, E. M., and SMITH, K., 1969, *J. chem. Phys.*, **51,** 3073.

[14] BROOKS, P. R., 1993, *J. phys. chem.*, **97,** 2153.

[15] HELBING, R. K. B., and ROTHE, E. M., 1968, *Rev. scient. Instrum.*, **39,** 1948.

[16] (*a*) HARLAND, P. W., CARMAN, H. S. JR., PHILLIPS, L. F., and BROOKS, P. R., 1989, *J. chem. Phys.*, **90,** 5201; (*b*) HARLAND, P. W., CARMAN, H. S. JR., PHILLIPS, L. F., and BROOKS, P. R.,1990, *Ibid.* **93,** 1089; (*c*) HARLAND, P. W., CARMAN, H. S. JR., PHILLIPS, L. F., and BROOKS, P. R., 1991, *J. phys. Chem.*, **95,** 8137.

[17] XING, G., KASAI, T., and BROOKS, P. R., 1995, *J. Am. chem. Soc.*, **117,** 2581.

[18] GANDHI, S. R., and BERNSTEIN, R. B.; 1988, *J. chem. Phys.*, **88,** 1472.

[19] BROOKS, P. R., 1973, *Faraday Disc. Chem. Soc.*, **55,** 299.

[20] ATEN, J., and LOS, J., 1975, *J. Phys.*, E, **8,** 408.

[21] KUNTZ, P. J., MOK, M. H., and POLANYI, J. C., 1969, *J. chem. Phys.*, **50,** 4623; HERSCHBACH, D. R., 1973, *Faraday Discuss. Chem. Soc.*, **55,** 233.

[22] BROOKS, P. R., MCKILLOP, J., and PIPPEN, H. G., 1979, *Chem. Phys. Lett.*, **66,** 144.

[23] CARMAN, H. S., HARLAND, P. W., and BROOKS, P. R., 1986, *J. phys. Chem.*, **90,** 944.
[24] (*a*) STOCKDALE, J. A., DAVIS, F. J., COMPTON, R. N., and KLOTS, C. E., 1974, *J. chem. Phys.*, **60,** 4279; (*b*) HENI, M., and ILLENBERGER, E., 1986, *Chem. Phys. Lett.*, **131,** 314.
[25] COMPTON, R. N., REINHARDT, P. W., and COOPER, C. D., 1978, *J. chem. Phys.*, **68,** 4360.
[26] KALAMARIDES, A., WALTER, C. W., LINDSAY, B. G., SMITH, K. A., and DUNNING, F. B., 1989, *J. chem. Phys.*, **91,** 4411; KALAMARIDES, A., MARAWAR, R. W., LING, X., WALTER, C. W., LINDSAY, B. G., SMITH, K. A., and DUNNING, F. B.,1990, *Ibid.*, **92,** 1672.
[27] (*a*) LOBO, R. F. M., MOUTINHO, A. M. C., and LOS, J., 1994, *Chem. Phys.*, **179,** 179; (*b*) LOBO, R. F. M., MOUTINHO, A. M. C., LACMANN, K., and LOS, J., 1991, *J. chem. Phys.*, **95,** 166.
[28] HASEGAWA, A., and WILLIAMS, F., 1977, *Chem. Phys. Lett.*, **46,** 66.
[29] MCNAMEE, P. E., LACMAN, K., and HERSCHBACH, D. R., 1973, *Faraday Discuss. Chem. Soc.*, **55,** 318.
[30] AITKEN, C. G., BLUNT, D. A., and HARLAND, P. W., 1994, *J. chem. Phys.*, **101,** 11074.
[31] FAIST, M. B., and LEVINE, R. D., 1976, *J. chem. Phys.*, **64,** 2953.